Multiferroic response to magnetic field in orthorhombic manganites

M. H. Qin,[1] Y. M. Tao,[2] S. Dong,[3] H. B. Zhao,[1] X. S. Gao,[1] and J.-M. Liu[1,2,4,a)]
[1]*School of Physics, South China Normal University, Guangzhou 510006, People's Republic of China*
[2]*Laboratory of Solid State Microstructures, Nanjing University, Nanjing 210093, People's Republic of China*
[3]*Department of Physics, Southeast University, Nanjing 211189, People's Republic of China*
[4]*International Center for Materials Physics, Chinese Academy of Science, Shenyang 110016, People's Republic of China*

(Received 5 January 2011; accepted 18 February 2011; published online 10 March 2011)

The magnetoelectric coupling in $Eu_{0.55}Y_{0.45}MnO_3$ is studied based on a microscopic spin model which includes the superexchange interaction, the single-ion anisotropy, the Dzyaloshinskii–Moriya interaction, and the cubic anisotropy. Our Monte Carlo simulation reproduces the experimentally observed multiferroic response to magnetic field B. It is demonstrated that the magnetic field can control the multiferroic behaviors by modulating the spin arrangements, leading to various flops of electric polarization. In addition, an interesting state in which both the electric polarizations along the a-axis and c-axis are activated under high B is predicted and discussed. © *2011 American Institute of Physics*. [doi:10.1063/1.3565241]

Multiferroics are attracting continuous attentions due to the interesting physics and potential applications.[1] In the past few years, multiferroicity has been found in a number of systems, such as spiral magnets, orthorhombically distorted perovskite manganites $RMnO_3$ [R=Tb, Dy, $Eu_{1-x}Y_x$, etc., crystal structure on the ab-plane is shown in Fig. 1(a)],[2] $Ni_3V_2O_8$,[3] $MnWO_4$,[4] and a conical magnet $CoCr_2O_4$.[5] The ferroelectricity in these materials is induced by spiral spin order through the inverse Dzyaloshinskii–Moriya (DM) mechanism (alternatively the spin current model).[6] In the spin current scenario, adjacent two spins (S_i,S_j) can generate a local polarization $P_{ij} \propto -e_{ij} \times (S_i \times S_j)$ with e_{ij} the unit vector connecting the two neighboring sites. Thus, polarization P in the ab-plane cycloidal spin (ab-CS) phase with propagation vector along the b-axis is induced along the a-axis while in the bc-plane cycloidal spin (bc-CS) phase it is induced along the c-axis, as illustrated in Figs. 1(b) and 1(c). $RMnO_3$ offers the capability for magnetic control of ferroelectricity via the strong magnetoelectric (ME) coupling. For $TbMnO_3$ and $DyMnO_3$, application of a magnetic field B along the b-axis (field B_b) flops P from the c-axis (polarization P_c) to the a-axis (polarization P_a).[7] Several theoretical works in order to understand the origin for such multiferroic response and the ME coupling in $RMnO_3$ are available.[8,9]

Most recently, a microscopic spin model (Mochizuki–Furukawa model) which includes the superexchange interaction, the single-ion anisotropy (SIA), the DM interaction, and the cubic anisotropy, was proposed and reproduced the phase diagrams of $RMnO_3$ in the plane of temperature (T) versus R-site ionic radius.[9] It was demonstrated that the orthorhombic lattice distortion mainly controlled by the R-ionic radius tunes the SIA and the DM interaction energies and in turn determines the competition between the ab-CS phase and bc-CS phase. This leads to the flop of P from the a-axis to the c-axis with reduced R-ionic radius. Subsequently, several other phenomena have been well explained based on the same or similar models.[10–14] For example, the phase diagrams of $TbMnO_3$ and $DyMnO_3$ under magnetic field B have been reproduced.[11]

On the other hand, several multiferroic states and strong ME effects were revealed in $RMnO_3$ (R=$Eu_{1-x}Y_x$) by tuning the R site ionic size.[15–17] In $Eu_{0.55}Y_{0.45}MnO_3$, polarization P flops from P_a to P_c when B is applied along the a-axis (B_a) while it flops from P_c to P_a with B along the c-axis (B_c) [see Figs. 1(d)–1(f)].[16] These ME phenomena may help us to understand the origin of the multiferroic response to B, due to the fact that this system is free from the influence of magnetic moments of R ions. Furthermore, a multiferroic state in which P is induced via the spin exchange striction mechanism was observed in $EuMnO_3$ under a field up to 30 Tesla (T).[10] It is thus reserved to question some unrevealed phases in $Eu_{0.55}Y_{0.45}MnO_3$ in the high B range.

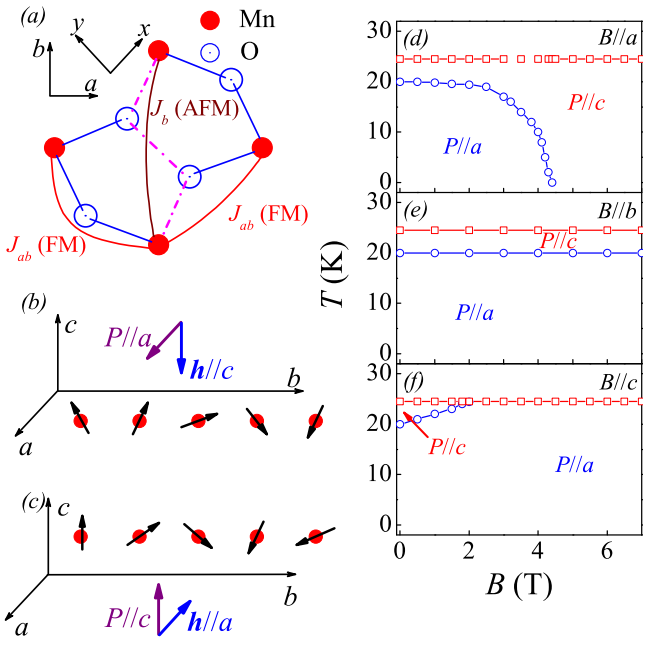

FIG. 1. (Color online) (a) Crystal structure (ab-plane) of $RMnO_3$. The induced P and spin-helicity vector $\boldsymbol{h}=\Sigma_{ij}S_i \times S_j$ in the ab-CS (b) and bc-CS (c) states. Experimentally obtained B-T phase diagrams for (d) $B \| a$, (e) $B \| b$, and (f) $B \| c$ are reproduced from Ref. 16.

a)Electronic mail: liujm@nju.edu.cn.

In this work, we study the Mochizuki–Furukawa model with Mn spin $S=2$ on a cubic lattice.[9] The Hamiltonian can be written as $H=H_{ex}+H_{\mathrm{SIA}}+H_{\mathrm{DM}}+H_{cub}+H_{\mathrm{Zeeman}}$. The first term $H_{ex}=\Sigma_{\langle i,j\rangle}J_{ij}\times(S_i\cdot S_j)$ denotes the spin exchange interactions, where $J_{ab}=-0.8$ and $J_b=0.8$ are the coupling constants in the Mn–Mn bonds on the *ab* plane [Fig. 1(a)], $J_c=1.25$ is the antiferromagnetic (AFM) exchange in the Mn–Mn bonds along the *c*-axis. Here the energy unit is millielectron volt. The second term is the SIA, which consists of two parts as $H_{\mathrm{SIA}}=D\cdot\Sigma_i S^i_{\zeta i}+E\cdot\Sigma_i(-1)^{i_x+i_y}\cdot(S^i_{\xi i}-S^i_{\eta i})$ with $D=0.25$, $E=0.30$. Here, ξ_i, η_i, ζ_i are the tilted local axes attached to the *i*th MnO_6 octahedron, as clearly given in Ref. 9. For their direction vectors, we use the experimental data of $EuMnO_3$.[18] The third term H_{DM} represents the DM interactions expressed by $H_{\mathrm{DM}}=\Sigma_{\langle i,j\rangle}d_{i,j}\times(S_i\times S_j)$. Here the DM vectors $d_{i,j}$ are determined by five DM parameters, $(\alpha_{ab},\beta_{ab},\gamma_{ab})=(0.10,0.10,0.14)$ and $(\alpha_c,\beta_c)=(0.30,0.30)$. The fourth term $H_{cub}=A\cdot\Sigma_i(S^4_{\mathrm{xi}}+S^4_{\mathrm{yi}}+S^4_{\mathrm{zi}})/S(S+1)$ represents the cubic anisotropy with coupling constant $A=0.0162$. The last term $H_{\mathrm{Zeeman}}=-B\mu_B g\Sigma_i S_i$ stands for the Zeeman coupling. Here $g=2$ is the Lande factor, and μ_B is the Bohr magneton.

Our Monte Carlo simulation is performed on a $36\times36\times6$ cubic lattice with periodic boundary conditions using the standard Metropolis algorithm and temperature exchange method.[19–21] The selected parameters reproduce well the magnetic states of $Eu_{0.55}Y_{0.45}MnO_3$ in the absence of *B*. With decreasing *T*, the system successively exhibits the paramagnetic (PM) phase, the sinusoidal collinear antiferromagnetic (sc-AFM) order with Mn spins along the *b*-axis, the *bc*-CS phase, and the *ab*-CS phase. The specific heat $C(T)=(\langle H^2\rangle-\langle H\rangle^2)/Nk_BT^2$ and spin-helicity vector $h_\gamma(T)=\langle|\Sigma_i S_i\times S_{i+b}|\rangle/NS^2$ $(\gamma=a,b,c)$ are calculated to determine the transition points and spin structures, here *N* is the number of Mn ions, k_B is the Boltzmann constant, and the brackets denote thermal and configuration averaging. The spin and spin-helicity correlation functions in the momentum space, $\Phi_\gamma(k,T)=\Sigma_{ij}\langle S_{\gamma i}\cdot S_{\gamma j}\rangle\exp[ik\cdot(r_i-r_j)]/N^2$ and $\Psi_\gamma(k,T)=\Sigma_{ij}\langle h^b_{\gamma i}\cdot h^b_{\gamma j}\rangle\exp[ik\cdot(r_i-r_j)]/N^2$ for $\gamma=a,b,c$ are also calculated in order to characterize the spin structures.

The calculated phase diagram in the *B*-*T* plane with $B\|a$-axis is shown in Fig. 2(a), which reproduces the observed *P* flop from the *a*-axis to the *c*-axis, in associated with the flop of the spiral-spin plane from the *ab*-plane to the *bc*-plane. In the low field range ($B_a=3.0$ T), the simulated $C(T)$ curve shows three specific-heat peaks, indicating the successive three phase transitions with decreasing *T*, as shown in Fig. 2(b). The first one is the transition from the PM phase to the sc-AFM phase. When *T* falls down to the second transition point, spin-helicity vector $h_a(T)$ increases while $h_b(T)$ and $h_c(T)$ remain small, fingering a transition to the *bc*-CS order. At the third transition, $h_c(T)$ steeply increases, accompanied with the sudden drop of $h_a(T)$, as a sign of spin spiral flop from the *bc*-plane to the *ab*-plane. In addition, the third transition point shifts toward the low-*T* side as B_a increases, indicating that the spiral-plane gradually flops from the *bc*-plane to the *ab*-plane at low *T*. As B_a increases up to 5 T and above, the system exhibits only two transitions at low *T*. For instance, at $B_a=6$ T, $C(T)$ shows two peaks and $h_a(T)$ is small over the whole *T*-range, as shown in Fig. 2(c). This simply indicates that the *bc*-CS order component if any is completely suppressed and the *ab*-CS order occupies the whole *T*-range below the second transition point, in agreement with experiments. It is well known that for an isotropic AFM or spiral spin system, field *B* tends to align the spins in perpendicular to *B*. The flop of spiral spin order into the *bc*-plane from the *ab* plane under high B_a becomes physically reasonable. Surely, such spiral-plane flop must be accompanied with the reorientation of *P*.

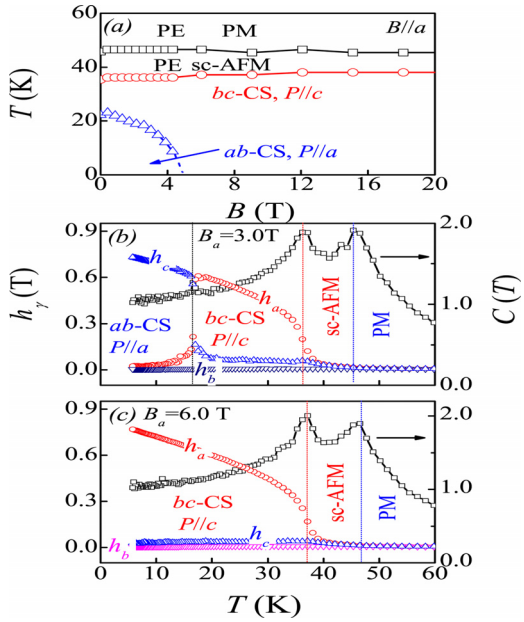

FIG. 2. (Color online) (a) Calculated B_a-*T* phase diagram of $Eu_{0.55}Y_{0.45}MnO_3$. Here, the high-temperature PM phase is denoted by PM, accompanied by the paraelectric phase PE, CS order denotes cycloidal spin order, sc-AFM stands for sinusoidal collinear antiferromagnetic order. Specific heat $C(T)$ and spin-helicity vector $h_\gamma(T)$ $(\gamma=a,b,c)$ as a function of *T* under various B_a: (b) $B_a=3.0$ T, and (c) $B_a=6.0$ T.

The effect of *B* on the multiferroicity revealed above also applies to the case with $B\|c$-axis (B_c). The calculated B_c-*T* phase diagram is displayed in Fig. 3(a). The magnetic field applied along the *c*-axis suppresses the *bc*-CS order while it enhances the *ab*-CS order, resulting in the flop of *P* from the *c*-axis to the *a*-axis. The *ab*-CS order overwhelms the *bc*-CS order at $B_c\sim3.0$ T, coinciding with experiments. For details, the calculated $C(T)$ and $h_\gamma(T)$ for $B_c=6.0$ T are shown in Fig. 3(b), indicating that the *ab*-plane spiral spin order is completely suppressed.

Subsequently, we look at the case of $B\|b$-axis (B_b). A prominent feature is that the magnetic phases in $Eu_{0.55}Y_{0.45}MnO_3$ show little dependence on B_b up to $B_b=7.0$ T, which is also reproduced in our simulation. At low field, the three magnetic transitions remain essentially unchanged and in fact no changes in the transition points (not shown here). One notes that for $RMnO_3$, the *ac*-CS order is unfavorable due to the fact that it cannot be stabilized by the DM interaction and the SIA. A low B_b cannot flip the spins into the *ac*-plane from the initial *ab*-plane and *bc*-plane, suggesting the robustness of the *ab*-CS or *bc*-CS orders. For high field case, as an example, we present the simulated $C(T)$ and $h_\gamma(T)$ at $B_b=9$ T in Fig. 3(c). The first and second transitions remain roughly unchanged while the third transition shifts toward the low-*T* side. In addition, below the second transition point, both $h_a(T)$ and $h_c(T)$ have large values, indicating the coexistence of the *bc*-CS order and the *ab*-CS

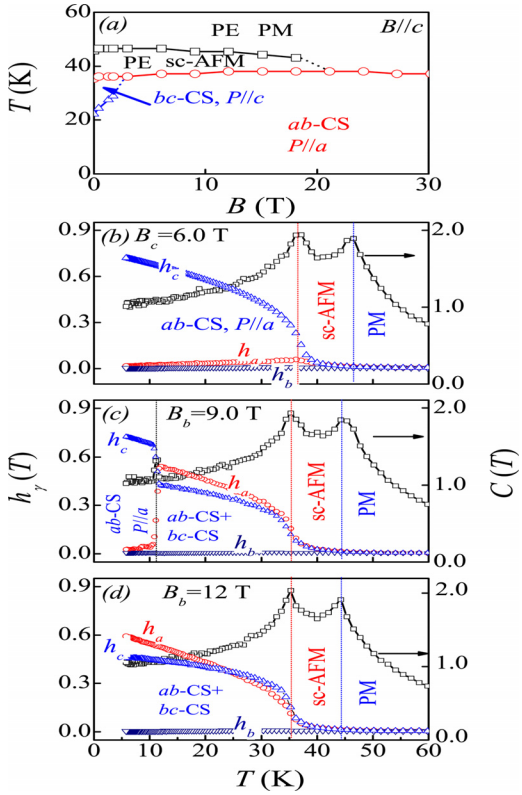

FIG. 3. (Color online) (a) Calculated B_c-T phase diagram. Specific heat $C(T)$ and spin-helicity vector $h_\gamma(T)$ as a function of T under: (b) B_c =1.3 T, (c) B_b=9.0 T, and (d) B_b=12 T.

order. In this case, the spins have both a-axis components and c-axis components. At the same time, the DM interaction with vectors on the in-plane Mn–O–Mn bonds stabilizes the ab-CS order while the DM interaction with vectors on the out-of-plane bonds stabilizes the bc-CS order. This leads to the simultaneous appearance of these two types of spiral spin orders. Around the third transition point, $h_a(T)$ suddenly drops to nearly zero, indicating the disappearance of the bc-CS order. As B_b increases up to 12 T, the system exhibits only two transitions, as shown in Fig. 3(d). The former is a transition from the PM phase into the sc-AFM phase, and the latter is a transition into a magnetic phase in which the ab-CS order and the bc-CS order coexist. According to the spin-current model, both P_a and P_c will be observed in the state with the coexisting ab-CS and bc-CS orders.

The Mochizuki–Furukawa model, proposed in the classical Heisenberg spin framework, shows surprisingly good consistency with experiments. In particular, our simulations reveal the coexistence of the ab-CS and bc-CS orders under high magnetic field along the b-axis, implying the coexistence of the a-axis and c-axis polarization components. In fact, the corresponding magnetic structures are also confirmed in our calculated spin-helicity correlations Ψ_γ. Figures 4(a) and 4(b) show the simulated $\Psi_\gamma(\gamma=a,c)$ under B_b=15 T at T=5 K. Both Ψ_a and Ψ_c have their peak locations at $k=(0,0,0)$, indicating the coexistence of the ab-CS and bc-CS orders. The simulated Φ_γ also characterize this spin structures. However, the predicted phase was not observed in earlier experiments in which the high field phase diagrams of $Eu_{1-x}Y_xMnO_3$(x=0 and 0.4) under B_b were studied in pulsed magnetic fields. This inconsistence between the theory and experiment may be due to the fact that the actual

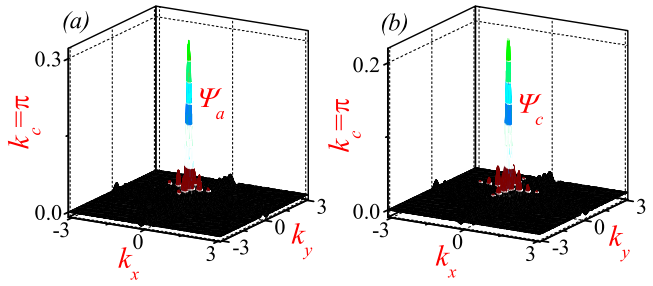

FIG. 4. (Color online) Calculated spin-helicity correlation functions (a) Ψ_a and (b) Ψ_c under B_b=15 T at T=5 K.

system is hard to be relaxed toward the equilibrium state at low T because of the high potential barrier between the equilibrium state and the quasi-static state under high B. Of course, this issue remains to be checked further.

This work was supported by the Natural Science Foundation of China (Grant Nos. 50832002, 51072061, 51031004, and 11004027), the National Key Projects for Basic Research of China (Grant No. 2011CB922101), and the China Postdoctoral Science Foundation (Grant No. 20100480768).

[1]M. Fiebig, J. Phys. D **38**, R123 (2005); W. Eerenstein, N. D. Mathur, and J. F. Scott, Nature (London) **442**, 759 (2006); Y. Tokura, J. Magn. Magn. Mater. **310**, 1145 (2007); S.-W. Cheong and M. Mostovoy, Nature Mater. **6**, 13 (2007); K. F. Wang, J.-M. Liu, and Z. F. Ren, Adv. Phys. **58**, 321 (2009).
[2]T. Kimura, T. Goto, H. Shintani, K. Ishizaka, T. Arima, and Y. Tokura, Nature (London) **426**, 55 (2003); T. Goto, T. Kimura, G. Lawes, A. P. Ramirez, and Y. Tokura, Phys. Rev. Lett. **92**, 257201 (2004).
[3]G. Lawes, A. B. Harris, T. Kimura, N. Rogado, R. J. Cava, A. Aharony, O. Entin-Wohlman, T. Yildirim, M. Kenzelmann, C. Broholm, and A. P. Ramirez, Phys. Rev. Lett. **95**, 087205 (2005).
[4]K. Taniguchi, N. Abe, T. Takenobu, Y. Iwasa, and T. Arima, Phys. Rev. Lett. **97**, 097203 (2006).
[5]Y. Yamasaki, S. Miyasaka, Y. Kaneko, J.-P. He, T. Arima, and T. Tokura, Phys. Rev. Lett. **96**, 207204 (2006).
[6]H. Katsura, N. Nagaosa, and A. V. Balatsky, Phys. Rev. Lett. **95**, 057205 (2005); M. Mostovoy, *ibid.* **96**, 067601 (2006); I. A. Sergienko and E. Dagotto, Phys. Rev. B **73**, 094434 (2006).
[7]T. Goto, Y. Yamasaki, H. Watanabe, T. Kimura, and Y. Tokura, Phys. Rev. B **72**, 220403(R) (2005); T. Kimura, Annu. Rev. Mater. Res. **37**, 387 (2007).
[8]S. Dong, R. Yu, S. Yunoki, J.-M. Liu, and E. Dagotto, Phys. Rev. B **78**, 155121 (2008).
[9]M. Mochizuki and N. Furukawa, J. Phys. Soc. Jpn. **78**, 053704 (2009); Phys. Rev. B **80**, 134416 (2009).
[10]M. Tokunaga, Y. Yamasaki, Y. Onose, M. Mochizuki, N. Furukawa, and Y. Tokura, Phys. Rev. Lett. **103**, 187202 (2009).
[11]M. Mochizuki and N. Furukawa, Phys. Rev. Lett. **105**, 187601 (2010).
[12]M. Mochizuki, N. Furukawa, and N. Nagaosa, Phys. Rev. Lett. **104**, 177206 (2010).
[13]M. Mochizuki and N. Nagaosa, Phys. Rev. Lett. **105**, 147202 (2010).
[14]M. Mochizuki, N. Furukawa, and N. Nagaosa, Phys. Rev. Lett. **105**, 037205 (2010).
[15]Y. Yamasaki, S. Miyasaka, T. Goto, H. Sagayama, T. Arima, and Y. Tokura, Phys. Rev. B **76**, 184418 (2007).
[16]H. Murakawa, Y. Onose, F. Kagawa, S. Ishiwata, Y. Kaneko, and Y. Tokura, Phys. Rev. Lett. **101**, 197207 (2008).
[17]S. Ishiwata, Y. Kaneko, Y. Tokunaga, Y. Taguchi, T. Arima, and Y. Tokura, Phys. Rev. B **81**, 100411(R) (2010).
[18]B. Dabrowski, S. Kolensnik, A. Baszczuk, O. Chmaissem, T. Maxwell, and J. Mais, J. Solid State Chem. **178**, 629 (2005).
[19]D. P. Landau and K. Binder, *A Guide to Monte Carlo Simulations in Statistical Physics* (Cambridge University Press, Cambridge, England, 2005).
[20]K. Hukushima and K. Nemoto, J. Phys. Soc. Jpn. **65**, 1604 (1996).
[21]M. H. Qin, X. Chen, and J.-M. Liu, Phys. Rev. B **80**, 224415 (2009).